Complex Vibrational Analysis of an Antiferroelectric Liquid Crystal Based on Solid-State Oriented Quantum Chemical Calculations and Experimental Molecular Spectroscopy

ARTICLE *in* THE JOURNAL OF PHYSICAL CHEMISTRY A · JUNE 2012

Impact Factor: 2.69 · DOI: 10.1021/jp301190z · Source: PubMed

6 AUTHORS, INCLUDING:

Edward Mikuli
Jagiellonian University
99 PUBLICATIONS **651** CITATIONS
SEE PROFILE

Antoni Kocot
University of Silesia in Katowice
80 PUBLICATIONS **1,093** CITATIONS
SEE PROFILE

THE JOURNAL OF PHYSICAL CHEMISTRY A

Article

pubs.acs.org/JPCA

Complex Vibrational Analysis of an Antiferroelectric Liquid Crystal Based on Solid-State Oriented Quantum Chemical Calculations and Experimental Molecular Spectroscopy

Kacper Drużbicki,*[,†,‡] Edward Mikuli,[†] Antoni Kocot,[§,∥] Mirosława Danuta Ossowska-Chruściel,[⊥] Janusz Chruściel,[⊥] and Sławomir Zalewski[‡,⊥]

[†]Department of Chemical Physics, Faculty of Chemistry, Jagiellonian University, Ingardena 3, 30-060, Cracow, Poland

[‡]Frank Laboratory of Neutron Physics, Joint Institute for Nuclear Research, 141980 Dubna, Russia

[§]Department of Biophysics and Molecular Physics, Institute of Physics, University of Silesia, Uniwersytecka 4, 40-007 Katowice, Poland

[∥]Department of Electronic and Electrical Engineering, Trinity College Dublin, Dublin 2, Ireland

[⊥]Department of Technology and Chemical Physics, Institute of Chemistry, University of Natural Sciences and Humanities, 3-go Maja 54, 08-110 Siedlce, Poland

Supporting Information

ABSTRACT: The experimental and theoretical vibrational spectroscopic study of one of a novel antiferroelectric liquid crystals (AFLC), known under the MHPSBO10 acronym, have been undertaken. The interpretation of both FT-IR and FT-Raman spectra was focused mainly on the solid-state data. To analyze the experimental results along with the molecular properties, density functional theory (DFT) computations were performed using several modern theoretical approaches. The presented calculations were performed within the isolated molecule model, probing the performance of modern exchange−correlations functionals, as well as going beyond, i.e., within hybrid (ONIOM) and periodic boundary conditions (PBC) methodologies. A detailed band assignment was supported by the normal-mode analysis with SQM ab initio force field scaling. The results are supplemented by the noncovalent interactions analysis (NCI). The relatively noticeable spectral differences observed upon Crystal to AFLC phase transition have also been reported. For the most prominent vibrational modes, the geometries of the transition dipole moments along with the main components of vibrational polarizability were analyzed in terms of the molecular frame. One of the goals of the paper was to optimize the procedure of solid-state calculations to obtain the results comparable with the all electron calculations, performed routinely for isolated molecules, and to test their performance. The presented study delivers a complex insight into the vibrational spectrum with a noticeable improvement of the theoretical results obtained for significantly attracting mesogens using modern molecular modeling approaches. The presented modeling conditions are very promising for further description of similar large molecular crystals.

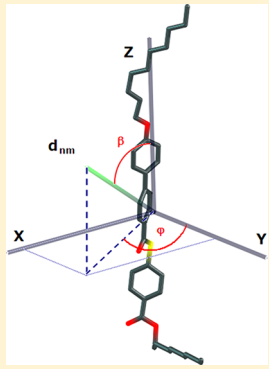

INTRODUCTION

It has been shown that vibrational spectroscopy of liquid crystals could be a very useful tool in a great number of phase transitions studies that can be investigated by both IR and Raman techniques. It has also been proven that the temperature dependent FT-IR spectroscopy of the aligned samples is an extremely valuable technique for exploration of the structure and order parameters in ferroelectric liquid crystals.[1−4] The similar studies, performed using Raman spectroscopy have been reported, e.g., by Fukuda and co-workers.[5−7] Two dimensional correlation analysis has also been proven to be a valuable supplementation of such experiments.[8,9] In all the cases an unambiguous knowledge of band assignment, their composition, and the related transition moment geometry is crucial. Because liquid crystal mesogens are one of the biggest size molecules studied by molecular orbitals calculations, the calculations were limited in quality for many years. Most commonly, the calculations were performed at the medium level of quality using isolated molecule model. Despite the fact that the size affects the complexity of the recorded spectra, such calculations very often deliver an excellent agreement with the experiment, especially when the studied systems are driven mainly by weak dispersive interactions.[10] However, the nature of the systems revealing spontaneous polarization may lead to the occurrence of more significant forces that result in a noticeable deviation with respect to the experimental data. Such an effect was observed for the title compound, giving doubts and raising a question: how reliable and unambiguous is the performed analysis?

Received: February 6, 2012
Revised: June 12, 2012
Published: June 18, 2012

   dx.doi.org/10.1021/jp301190z | J. Phys. Chem. A 2012, 116, 7809−7821

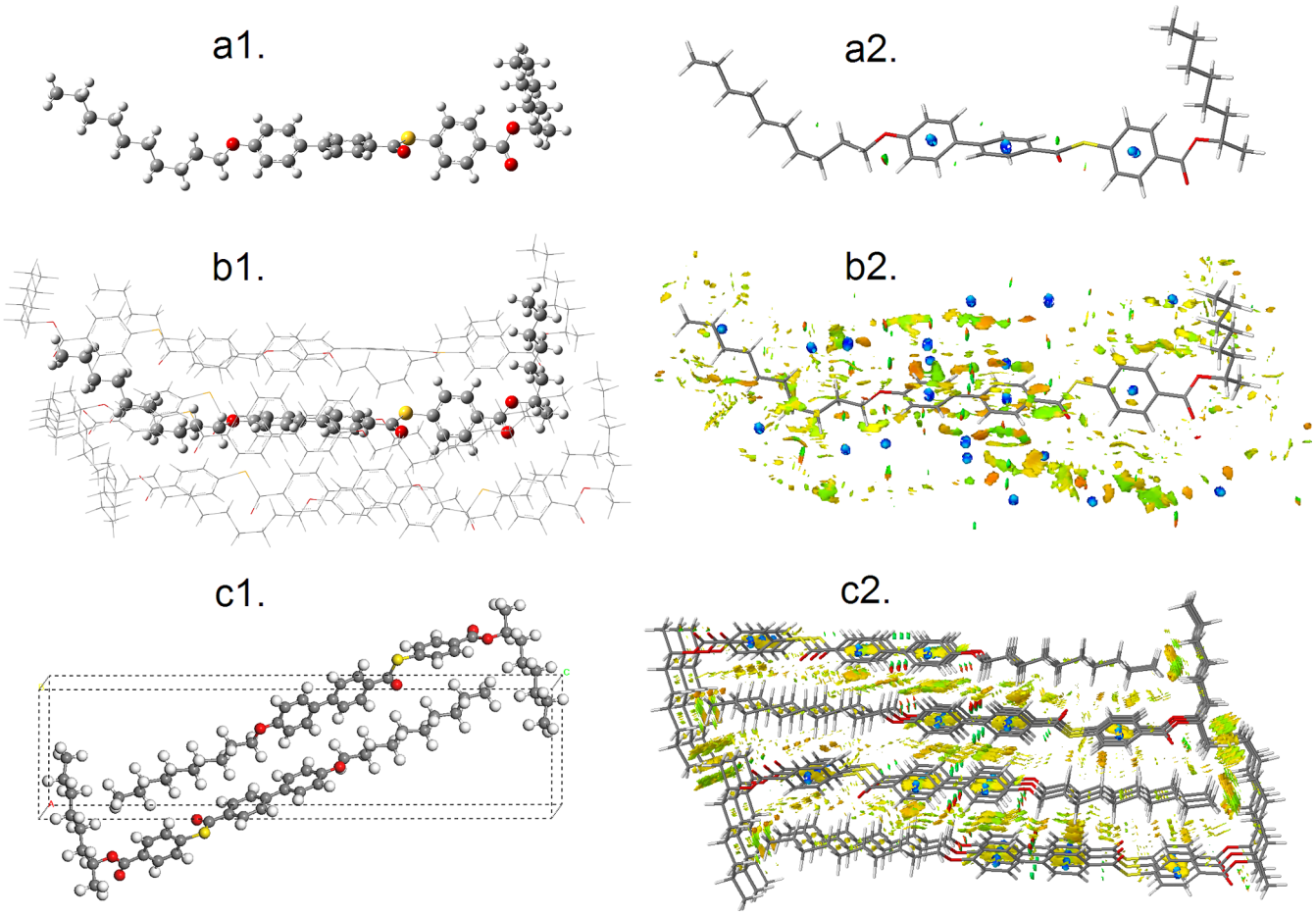

Figure 1. Equilibrium molecular geometries of MHPSBO10 delivered by the following theoretical models: (a1) isolated molecule, PBE/6-31+G(d); (b1) ONIOM-PBE/+6-31G(d):PBE/3-21G(d); (c1) PBE/NC-PW:1050eV. Corresponding NCI analysis isosurfaces (a2, b2, c2). The isosurfaces plotted with the density cutoff = 0.25.

The main goal of this paper is to deliver a detailed vibrational analysis of one of a novel antiferroelectric liquid crystals, with the full name (*S*)-1-methylheptyl-4-(4′-decyloxybiphenylthiocarboxy)benzoate, also known as MHPSBO10. Furthermore, we shed light on the performance and accuracy of the modern quantum-chemical models, trying to answer the question if any improvement is possible and confirm an appropriateness of the proposed band assignment.

The temperature dependent FT-IR studies of the title compound are the topic of a separate paper and will be presented in detail elsewhere.[11] The results were limited here to the middle range of frequencies (3250−550 cm^{-1}), due to its most applicable potential. The analysis of the low-frequency vibrational spectrum, in the context of the crystalline structure and the solid-state polymorphism, is also out of interest of the present work and will be discussed in another paper.[12]

CHARACTERISTIC OF MHPSBO10

The details of the synthesis along with the basic data concerning polymorphism of the title compound have been recently published by Ossowska et al.[13] MHPSBO10 belongs to the homologous series of (*S*)-MHPSBO*n*, which is analogous to the family of the first known antiferroelectric compound MHPOBC, differing in the replacement of the ester group by the more soft thioester bridge.[13] The (*S*)-MHPSBO*n* series differs in the number of carbon atoms in the achiral alkyl chain, which varies from n = 7 to 10. The molecular structure of the title compound is presented in Figure 1a and will be discussed in the next chapter.

The compound reveals very rich polymorphism, including both ferro-smectic (SmC*), antiferro-smectic (SmC^*_A, SmI^*_A), and paraelectric (SmA*) smectic phases. As for the highest homologous compound in the series, the phase transitions in MHPSBO10 may be observed at the lowest temperatures. No ferrielectric subphases were detected here. The phase situation of MHPSBO10, determined using differential scanning calorimetry (DSC), with the heating/cooling rate of 2 °C/min, may be presented as follows:

$$\text{Cooling}\quad \text{Iso} \xrightarrow{165.4\,^\circ\text{C}} \text{SmA}^* \xrightarrow{153.2\,^\circ\text{C}} \text{SmC}^* \xrightarrow{142.9\,^\circ\text{C}} \text{SmC}^*_\text{A} \xrightarrow{85.6\,^\circ\text{C}} \text{SmI}^*_\text{A} \xrightarrow{19.6\,^\circ\text{C}} \text{Cr}$$

$$\text{Heating}\quad \text{Cr} \xrightarrow{83.0\,^\circ\text{C}} \text{SmI}^*_\text{A} \xrightarrow{86.3\,^\circ\text{C}} \text{SmC}^*_\text{A} \xrightarrow{144.3\,^\circ\text{C}} \text{SmC}^* \xrightarrow{153.8\,^\circ\text{C}} \text{SmA}^* \xrightarrow{166.2\,^\circ\text{C}} \text{Iso}$$

The rich polymorphism makes the compound an interesting object of many physicochemical studies. The complex studies of the mesomorphic properties have been performed using many complementary techniques, namely differential scanning calorimetry (DSC), polarization microscopy (POM), transmitted light intensity (TLI) measurements, electrooptical methods, dielectric spectroscopy, and others, and have been presented in detail elsewhere.[14]

dx.doi.org/10.1021/jp301190z | J. Phys. Chem. A 2012, 116, 7809−7821

Because the structure of the title compound is not fully resolved yet, the studies were partially based on the X-ray data recorded for the analogous MHPSBO8 single crystal, which differs in the length of the achiral chain.[15] The powder XRD studies at room temperature confirmed that the title compound crystallizes in the P_{21} point group, with $Z = 2$.[12] The validity of the assumed molecular configuration was confirmed by a full unrestricted optimization with periodic boundary conditions (PBC) using the COMPASS force field as implemented in Discover module of Materials Studio 5.5.[16,17] package. The results revealed an excellent agreement with the experimentally determined cell parameters and such configuration was taken for further consideration.

EXPERIMENTAL AND COMPUTATIONAL METHODS

Experimental Details. The compound was synthesized and optically purified by Ossowska-Chrusciel as presented in the original paper.[13] The vibrational spectra were recorded for the unaligned samples. Due to relatively most noticeable changes induced by the solid → AFLC transition, the report was restricted to the spectra recorded in both phases. The FT-IR spectra were recorded in the range 4000−550 cm^{-1}, with spectral resolution of 2 cm^{-1} and accumulation of 32 scans using a Nicolet Magna 760 spectrometer, equipped with a DTGS detector, KBr beamplitters, and a Globar infrared source. The ZnSe 10.2 μm thick cell was filled by capillary forces in the isotropic phase and cooled to the crystalline state. To check possible differences arising from the surface effects, the attenuated total reflectance (ATR) spectrum of the polycrystalline sample has been also recorded, with the same measurements conditions, using FT-IR Varian 670 spectrometer, equipped with IR 670 microscope, germanium crystal, and MCT FPA detector. The FT-RS measurements were performed using a Bruker RamScope III spectrometer, with the 1064 nm excitation line of Nd:YAG laser and germanium detector. The laser power of 100 mW, spectral resolution of 2 cm^{-1}, and the accumulation of 128 scans were chosen as the experimental conditions. A Linkam 600 heating stage was used to record the Raman spectrum in the AFLC phase. The signal was directed into the Raman microscope via an optical fiber. The presented spectra were analyzed here, down to 550 cm^{-1}, in the range that is most interesting from the point of view of further spectroscopic studies. The low range spectra will be presented and analyzed along the XRD studies which are in progress.[12]

Computational Details. The isolated molecule computations were done with Gaussian 09 rev B.1.[18] The computations were performed using several theoretical models including the most popular exchange−correlation functionals with 6-31+G(d,p) basis set. The direct spectral comparison is presented in the Supporting Information. Some calculations were repeated with 6-31+G(d) as well as with triple-ζ quality 6-311+G(d,p) basis set. The double-ζ quality 6-31+G(d) level proved to be good enough in the description of the studied spectrum. The B3LYP results were treated as a standard.[19−22] To improve the calculated spectrum, the scaled quantum mechanical (SQM) force field procedure was applied at the B3LYP/6-31+G(d) level, using the refined scale factors proposed by Korlacki et al.[23] who has shown that the quoted set performs extremely well in the description of the ferroelectric thiobenzoates. The cited scale factors were applied without any further refinement. The SQM-ff based normal-mode analysis was performed using the MOLVIB program ver. 7.1., written by Sundius[24,25] based on Pulay's method.[26] The constructed symmetry coordinate definitions are provided in the Supporting Information.

Because the ferroelectric liquid crystalline systems are driven significantly by intermolecular interactions, we have also tried to check the potential improvement when going beyond the isolated molecular model. The polarizable continuum model (PCM) calculations, using benzene as a solvent, did not deliver any significant advantage. Hence, we have tried to mimic the close environment *explicite* by applying the cluster model within the hybrid ONIOM approach as developed by Morokuma and co-workers.[27] In that purpose we have built the molecular cluster, where the central mesogen is hexagonaly surrounded by six molecules giving the possibly uniform distribution of the electron density. The low layer was treated with universal force field (UFF) and Merz−Singh−Kollman partial charges electron embedding. However, several tests for the low layer description, including usage of semiempirical methods (AM1, PM3, and PM6), have shown that some advantage may be observed only when a more sophisticated theory level is used. Several basis sets were also tested, including use of pseudopotentials, and we may conclude that an observable improvement may be achieved only when using nonminimal basis sets, at least 3-21G(d). Because the benchmark calculations have proven that PBE functional delivered practically the same accuracy as more sophisticated hybrid functionals, the central molecule was described with PBE/6-31+G(d).[28,29] Moreover, choosing PBE has an advantage of no need of using drastic scaling procedures, which makes the comparison of different models more consistent.[30] Thus, the final calculations were performed with the PBE/6-31+G(d):PBE/3-21G(d) level. Unfortunately, due to memory allocation errors, which occurred in vibrational analysis due to the system size, we had to limit the PBE/3-21G(d) description to the mesogenic cores and calculate the normal modes by describing the alkyl fragments in the surrounding part with the UFF force field. The vibrational analysis was focused only on the high layer, hence the normal modes were computed and analyzed only for the uniformly surrounded central molecule. The band assignment was based on the normal modes visualization with the CHEMCRAFT program.[31]

Finally, we have performed the solid-state DFT computations for the previously described crystal structure. The computations were performed using the Materials Studio 5.5 suite of programs, with DMOL3 and CASTEP (the results not presented here) and using the QUANTUM ESPRESSO (QE) package.[32−35] As the studied unit cell consists of 186 nonexotic atoms and no drastic changes in the electron density are expected, all the calculations were performed only at the Γ point of the Brillouin zone.

The DMOL3 computations were performed at the PBE/DNP level. The experimentally determined cell parameters were fixed during the optimization and only the internal coordinates were relaxed with ultrafine convergence tolerance. Actually there is no way to compute the corresponding Raman intensities with DMOL3 (up to the actually available version 5.5). Moreover, the only approximate way to compute the infrared intensities is to use the so-called differential dipoles method developed by Korter et al.[36] Hence, we have calculated the intensities using Hirshfeld charges at the quoted theory level with the Perl script written by Fitzgerald.[37] Although the all electron solid-state calculations performed with DMOL3 sufficiently reproduces the mode frequencies, the intensities

dx.doi.org/10.1021/jp301190z | J. Phys. Chem. A 2012, 116, 7809−7821

Table 1. Analysis of the Experimental IR and RS Spectra of MHPSBO10 Recorded for Crystal and AFLC States[a]

IR crystal	RS Cr crystal	IR AFLC	RS AFLC	SQM B3LYP	SQM PED contributions [≥5%]
	3077 w			3091	$\nu_{ss}CH_{Ph}{}^{c}$[99]
	3067 w		3071 vw	3087	$\nu_{ss}CH_{Ph}{}^{c}$[99]
3060 vw		3059 vw		3085	$\nu_{ss}CH_{Ph}{}^{a}$[98]
	3051 vw		3055 vw	3073	$\nu_{ss}CH_{Ph}{}^{b}$[59], $\nu_{ss}CH_{Ph}{}^{a}$[36]
3045 vw		3047 vw		3073	$\nu_{ass}CH_{Ph}{}^{c}$[95]
3033 vw	3034 w	3033 vw	3041 vw	3051	$\nu_{ass}CH_{Ph}{}^{a}$[77], $\nu_{ass}CH_{Ph}{}^{b}$[22]
2978 w	2982 w	2978 w	2988 w	2955	$\nu_{ips}CH_{3}{}^{b}$[95]
2959 st	2959 w	2959 st	2960 w	2939	$\nu_{ops}CH_{3}{}^{b}$[83], νC*—H[12]
	2935 w		2934 w	2864−2902	$\nu_{ass}CH_{2}$[93−99]
2931 vst		2929 vst			
	2907 w		2916 w		
2901 st		2901 st			
	2887 w		2898 w	2861	$\nu_{ss}CH_{3}$[98]
2871 st		2873 st		2860	
2855 st		2856 st		2832−2855	$\nu_{ss}CH_{2}$[99]
	2866 w		2871 w		
	2849 w		2851 w		
1714 st	1714 w	1719 st	1719 w	1701	νC═O^{b}[75], δPh^{c}—C—O[8], νPh^{c}—C[5]
1675 vst	1676 w	1678 vst	1677 w	1685	νC═O^{a}[82], δPh^{b}—C—S[5]
1607 vw				1610	νCCPh^{a}[50], ρPh^{a,b}—X[22], νCCPh^{b}[14], βPh$^{a}_{symd}$[9]
1600 st	1595 vst	1599 st	1596 vst	1596	νCCPh^{b}[46], ρPh^{a,b}—X[22], νCCPh^{a}[13], βPh$^{b}_{symd}$[9]
1580 vw		1578 vw		1593	νCCPh^{c}[62], ρPh^{c}—X[22], βPh$^{c}_{symd}$[11]
1561 w	1559 vw	1559 w	1558 vw	1545	νCCPh^{b}[49], ρPh^{a,b}—X[20], νCCPh^{a}[18], βPh$^{b}_{asymd}$[7]
1527 m	1530 vw	1523 m	1525 vw	1515	ρPh^{a,b}—X[48], νCCPh^{a}[20], νCCPh^{b}[12], νCC_{biPh}[9]
1496 m	1494 vw	1494 m	1497 vw	1493	ρPh^{a,b}—X[59], νCCPh^{b}[20], νCCPh^{a}[10]
1473 m	1474 vw	1472 m	1476 vw	1474	$\delta CH_{2}{}^{a}$[92]
1466 m		1467 m		1469	$\delta CH_{2}{}^{b}$[82], $\delta_{ipb}CH_{3}{}^{c}$[15]
	1460 vw		1456 vw	1458	$\delta CH_{2}{}^{a}$[85], $\delta_{ipb}CH_{3}{}^{a}$[8]
1453 w		1456 w		1458	$\delta_{opb}CH_{3}{}^{c}$[92], $\rho_{opr}CH_{3}{}^{c}$[8]
	1449 vw		1443 vw	1453	$\delta CH_{2}{}^{b}$[63], $\delta_{ipb}CH_{3}{}^{c}$[30]
1440 vw		1444 vw		1449	$\delta_{opb}CH_{3}{}^{b}$[61], $\delta_{ipb}CH_{3}{}^{b}$[13], $\delta CH_{2}{}^{b}$[12], $\rho_{opr}CH_{3}{}^{b}$[6]
	1438 vw		1436 vw	1447	$\delta CH_{2}{}^{a}$[92]
1427 vw	1430 vw		1426 vw	1420	ρPh^{a,b}—X[45], νCCPh^{a}[31], νCCPh^{b}[14]
1400 st	1394 vw	1398 st	1397 vw	1387	ρPh^{c}—X[39], νCCPh^{c}[34], ρ_{ipr}C*[11], ρ_{opr}C*[6]
1391 m		1385 m		1380	$\omega CH_{2}{}^{a}$[77], $\nu CC_{alk}{}^{a}$[15]
1375 w	1372 vw	1379 w		1367	$\delta_{sb}CH_{3}{}^{b}$[73], ρ_{ipr}C*[10], $\nu CC_{alk}{}^{b}$[6]
1348 w	1350 vw	1356 w	1355 vw	1348	$\omega CH_{2}{}^{a}$[79], $\nu CC_{alk}{}^{a}$[13]
1326 w	1326 vw		1327 w	1315	ρPh^{a,b}—X[58], νCCPh^{b}[18], νCCPh^{a}[14]
1314 m		1312 m		1305	νCCPh^{c}[47], ρPh^{c}—X[45]
1308 m	1312 vw		1310 vw	1300	νCCPh^{a}[39], νCCPh^{b}[34], ρPh^{a,b}—X[18]
	1296 vw		1294 vw	1284	$\tau CH_{2}{}^{a}$[74], $\omega CH_{2}{}^{a}$[18], $\rho CH_{2}{}^{a}$[5]
1292 vst		1289 vst		1269	$\omega CH_{2}{}^{b}$[59], νCCPh^{b}[10], νCCPh^{a}[7]
	1284 m		1284 m	1275	νCC_{biPh}[40], ρPh^{a,b}—X[21], βPh$^{a}_{trigd}$[9], βPh$^{b}_{trigd}$[8], νCCPh^{b}[8], νCCPh^{a}[6]
1276 vst	1273 vw	1272 vst	1273 vw	1257	νPh^{c}—C[26], νC—O^{b}[25], ρC═O^{b}[12], νCCPh^{c}[10], $\tau CH_{2}{}^{b}$[6], ρ_{ipr}C*[5]
1257 st	1258 w	1252 st	1252 w	1243	νC—O^{a}[35], νCCPh^{a}[31], $\tau CH_{2}{}^{a}$[14], ρPh^{a,b}—X[7]
1245 w		1240 w		1249	$\tau CH_{2}{}^{a}$[42], $\omega CH_{2}{}^{a}$[29], $\rho CH_{2}{}^{a}$[13], νC—O^{a}[6]
1223 vw	1224 vw	1214 vw	1214 vw	1202	ρPh^{a,b}—X[38], νCCPh^{b}[24], νPh^{b}—C[23], βPh$^{b}_{trigd}$[7]
1189 vst		1185 vst		1174	ρPh^{c}—X[73], νCCPh^{c}[21]
1181 st	1183 vst	1178 st	1179 vst	1169	ρPh^{a,b}—X[38], vPh^{b}—C[23], νCCPh^{b}[14], βPh$^{b}_{trigd}$[5]
1148 w		1144 w		1140	$\rho CH_{2}{}^{b}$[45], $\nu CC_{alk}{}^{b}$[14], $\rho_{opr}CH_{3}{}^{b}$[9], δ_{sb}C*[7], $\rho_{opr}CH_{3}{}^{c}$[5]
	1129 vw			1121	$\nu CC_{alk}{}^{b}$[25], $\delta CCC_{alk}{}^{b}$[23], $\rho_{ipr}CH_{3}{}^{c}$[10], $\rho CH_{2}{}^{b}$[10], $\tau CH_{2}{}^{b}$[6]
1122 m	1120 vw	1115 m	1123 vw	1117	ρPh^{a,b}—X[59], νCCPh^{b}[33]
1116 st				1105	ρPh^{c}—X[35], νCCPh^{c}[24], νC—O^{b}[17], βPh$^{c}_{trigd}$[6]
1108 st		1105 st		1094	ρPh^{c}—X[30], νC—O^{b}[27], νCCPh^{c}[25], βPh$^{c}_{trigd}$[7]
1096 m	1093 vw	1091 m	1091 vw	1070	νCCPh^{c}[52], νC—S[22], νC—O^{b}[6]
1066 vw	1065 vw	1058 vw	1066 vw	1049	$\nu CC_{alk}{}^{a}$[80], $\tau CH_{2}{}^{a}$[8]
1057 vw				1064	$\nu CC_{alk}{}^{a}$[73], $\tau CH_{2}{}^{a}$[7], νC—O^{a}[7]
1048 vw	1048 vw	1045 vw	1047 vw	1031	$\nu CC_{alk}{}^{b}$[91], $\tau CH_{2}{}^{b}$[6]
1040 vw		1035 vw		1027	$\nu CC_{alk}{}^{a}$[31], νC—O^{a}[29], νCCPh^{b}[7], $\omega CH_{2}{}^{a}$[6], νCCPh^{a}[6]
1031 vw		1030 vw		1017	βPh$^{c}_{trigd}$[60], νCCPh^{c}[26], ρPh^{c}—X[9]
1018 st	1018 vw		1019 vw	1013	νCCPh^{b}[36], βPh$^{b}_{trigd}$[31], ρPh^{a,b}—X[13], νC—O^{a}[7]

dx.doi.org/10.1021/jp301190z | J. Phys. Chem. A 2012, 116, 7809−7821

Table 1. continued

IR crystal	RS Cr crystal	IR AFLC	RS AFLC	SQM B3LYP	SQM PED contributions [≥5%]
1015 w		1017 st		1004	τCH_2^b[41], νCC_{alk}^b[26], $\rho_{ipr}CH_3^b$[8]
999 w	993 vw	999 w		995	$\nu CCPh^a$[15], νCC_{alk}^a[15], τCH_2^a[15], $\nu C—O^a$[14], βPh^a_{trigd}[10], $\nu CCPh^b$[7]
994 w		989 w		984	νCC_{alk}^b[68], τCH_2^b[14], $\nu C—O^b$[7]
982 vw				977	νCC_{alk}^b[58], δCCC_{alk}^b[13], $\rho_{ipr}CH_3^c$[10], ωCH_2^b[6]
959 vw		956 vw		955	τCH_2^a[41], ρCH_2^a[25], νCC_{alk}^a[22], $\rho_{opr}CH_3^a$[6]
	963 vw		962 vw	952	$\gamma Ph^{a,b}—X$[83], γPh^b_{trig}[11]
	932 vw			917	νCC_{alk}^a[30], ρCH_2^a[26], τCH_2^a[26], δCCC_{alk}^a[7]
920 w	925 vw	920 w	925 vw	900	νCC_{alk}^b[33], $\rho_{opr}CH_3^b$[23], $\nu C—O^b$[18], $\rho_{ipr}CH_3^b$[10]
905 vst	905 vw	903 vst	903 vw	887	$\rho C=O^a$[33], $\nu CCPh^b$[23], $\nu C—S$[15], $\nu Ph^b—C$[11], βPh^b_{trigd}[8]
900 m	890 vw	895 m	887 vw	878	ρCH_2^a[36], ωCH_2^a[23], νCC_{alk}^a[16], $\rho_{opr}CH_3^a$[12], δCCC_{alk}^a[5]
883 vw	874 vw		864 vw	868	ρCH_2^b[23], ωCH_2^b[16], νCC_{alk}^b[11], $\rho_{opr}CH_3^c$[9], $\rho_{ipr}CH_3^b$[6], $\delta C—O—C^a$[5]
855 m		852 m		852	$\gamma Ph^{a,b}—X$[73], $\gamma Ph^b—biPh$[8], γPh^b_{sym}[7]
850 vw	855 vw		853 vw	848	$\gamma Ph^c—X$[77], $\omega C=O^b$[12], γPh^c_{sym}[10]
839 vw		834 vw		840	ρCH_2^a[62], τCH_2^a[12], $\gamma Ph^{a,b}—X$[9], νCC_{alk}^a[6]
	840 vw		839 vw	829	$\gamma Ph^{a,b}—X$[83]
824 st		824 st		818	$\gamma Ph^{a,b}—X$[87]
	830 vw		828 vw	816	$\nu CCPh^a$[26], $\nu C—O^a$[16], βPh^a_{symd}[13], ρCH_2^a[11], $\gamma Ph^{a,b}—X$[7], νCC_{alk}^a[6]
817 st	819 vw	820 st	814 vw	801	$\gamma Ph^{a,b}—X$[73], ρCH_2^a[13]
806 vw	803 vw	806 vw	802 vw	792	ρCH_2^a[54], $\gamma Ph^{a,b}—X$[16], τCH_2^a[14], $\rho_{opr}CH_3^a$[8]
763 st		762 st		759	$\gamma Ph^c—X$[38], $\omega C=O^b$[30], γPh^c_{trig}[27]
741 m		744 m		743	ρCH_2^a[67], τCH_2^a[19], T_{alk}[5]
736 st	736 w	734 st	743 w	731	βPh^b_{symd}[27], $\nu CCPh^b$[11], $\rho C=O^a$[10], ρCH_2^a[9], νCC_{biPh}[6], $\nu C—S$[6]
729 m		731 m		723	βPh^c_{symd}[43], $\nu C—S$[17], $\rho C=O^b$[12], $\nu\nu CCPh^c$[10]
713 vw		716 vw		702	ρCH_2^a[82], T_{alk}[15]
693 m	692 vw	692 m	687 vw	682	γPh^c_{trig}[66], $\gamma Ph^c—X$[23], $\omega C=O^b$[8]
647 vw				649	βPh^a_{asymd}[39], βPh^b_{asymd}[35]
642 vw	641 vw	650 vw	647 vw	643	βPh^b_{asymd}[18], $\omega C=O^a$[14], βPh^a_{asymd}[9], βPh^a_{symd}[8], $\gamma Ph^{a,b}—X$[7], $\rho Ph^{a,b}—X$[6]
640 vw		643 vw		639	βPh^c_{asymd}[81], $\nu CCPh^c$[8]
624 vw	625 vw	625 vw	628 vw	630	βPh^b_{asymd}[20], βPh^a_{symd}[18], βPh^a_{asymd}[13], βPh^b_{symd}[7], $\delta C—O—C^a$[6], $\rho C=O^a$[5]
575 w	576 vw	575 w	574 vw	566	$\delta Ph^b—C—S$[19], $\nu C—S$[13], $\delta C—S—Ph^c$[11], $\gamma Ph^c—X$[8], γPh^c_{trig}[7], $\rho Ph^{a,b}—X$[7]

[a]The band assignment was based on the SQM B3LYP/6-31+G(d) normal mode analysis. Table legend: relative percentage intensity: vw, 0−5% ; w, 5−15% ; m, 15−30%; st, 30−60%; vst, 60−100%. Symmetry coordinates notation: ν, stretching; δ, bending; τ, twisting; ω, wagging; ρ, rocking; T, torsion; β, in-plane; γ, out-of-plane. Superscript a, b, c are labels denoting the molecular parts (see the Supporting Information for details).

prediction in the midfrequency range has completely failed with the cited approximation. It made the obtained results partially worthless, due to the 555 ($3N - 3$) normal modes calculated with improperly predicted intensities. The band assignment for the DMOL3 results was based on the visualization of the normal modes using J-ICE program.[38,39]

The only way of solving the intensities problem is to apply density functional perturbation theory (DFPT).[40] The QUANTUM ESPRESSO (QE) calculations were performed with the same optimization scheme, within the plane-wave methodology, norm-conserving pseudopotentials and PBE functional. A significantly large kinetic energy cutoff of 1050 eV was used to minimize the basis set errors. We have performed a test for several available sets of norm-conversing pseudopotentials constructed for PBE, which have proven that the Troullier−Martins type ones developed by Bennett and Rappe tend to be superior in the description of the studied system and may be highly recommended for similar studies.[41] The sulfur atoms were described by the core-corrected pseudopotential generated using ATOMIC code by Dal Corso (QE distribution).[42] The optimization was performed with the 1.0×10^{-6} threshold convergence of the Hellmann−Feynman forces. The geometry optimization was followed by vibrational analysis within DFPT using gamma-point algorithms and the 1.0×10^{-14} threshold convergence for phonon calculations.[40] "Simple" type acoustic sum rule (ASR) was imposed. It should be underlined that we were unable to obtain the Raman activities using PBE functional, because the higher derivatives calculations are not yet available for GGA approach up to present 4.3.2 version of QE. Thus, due to the high accuracy of the computed infrared spectrum, the RS activities were computed for the corresponding geometry with no further optimization using local density approximation (LDA), with Perdew−Zunger functional (PZ-LDA) and the norm-conserving pseudopotentials generated with ATOMIC code.[43,42] Although such an approach is not strictly theoretically justified, it has delivered a very good relation of intensities with respect to the experiment, as may be seen below. To get the intensities for such a tidy system, the DYNMAT code was modified in such way that it does not use large automatic arrays of memory, and allocates only those arrays that are actually needed.[44] The obtained RS activities were finally transformed into the intensities using the well-known relation derived from the theory of Raman scattering.The band assignment was based on the normal modes visualization using MOLDEN program.[45]

The infrared calculations were repeated using CASTEP code, with the same numerical conditions, the quoted Bennett and Rappe pseudopotentials and the remaining one for the sulfur atom taken from the Materials Studio 5.5 repository (developed by the Ming-Hsien Lee's Group).[46] The obtained results are of very comparable accuracy. Application of the empirical dispersion corrections also did not bring any noticeable improvement in the studied case.

Table 2. Analysis of the Most Prominent and Applicable Bands Observed in the Vibrational Spectrum of MHPSBO10[a]

							IR		RS		
FT-IR [cm^{-1}]	FT-RS [cm^{-1}]	B3LYP/ SQM [cm^{-1}]	PBE/ISO [cm^{-1}]	PBE/ ONIOM [cm^{-1}]	PBE/ DMOL3 [cm^{-1}]	PBE/QE [cm^{-1}]	β^{μ} [deg]	φ^{μ} [deg]	β^{α} [deg]	φ^{α} [deg]	PED > 10% [%]
1714	1714	1701	1709	1680	1713	1680	59.4	57.8	65.5	68.4	νC═O^{b}[75]
1675	1676	1685	1700	1665	1663	1647	69.3	128.0	78.8	58.7	νC═O^{a}[82]
1600		1596	1602	1591	1583 (oop)	1579 (oop)	177.9	75.2	0.1	86.0	νCCPh^{b}[46], ρPh$^{a,\,b}$—X[22], νCCPh^{a}[13]
	1595				1577 (ip)	1573 (ip)					
1527	1530	1515	1518	1525	1516	1515	6.7	131.4	0.6	52.2	ρPh$^{a,\,b}$—X[48], νCCPh^{a}[20], νCCPh^{b}[12]
1189		1169	1211	1187	1216	1164	170.6	133.0	1.1	49.1	ρPh^{c}—X[73], νCCPh^{c}[21]
1181	1183	1174	1174	1179	1175	1172	173.1	83.7	0.8	89.3	ρPh$^{a,\,b}$—X[38], vPh^{b}—C[23], νCCPh^{b}[14]
1108		1094	1091	1098	1092	1101	152.3	30.1	12.3	18.6	ρPh^{c}—X[30], νC−O^{b}[27], νCCPh^{c}[25]
	1093	1070	1081	1083	1098	1094	114.1	6.1	78.5	0.6	νCCPh^{c}[52], νC—S[22]
905		887	881	887	893	893	160.4	116.8	5.6	75.7	ρC═O^{a}[33], νCCPh^{b}[23], νC—S[15], vPh^{b}—C[11]
763		759	743	749	756	783	65.5	165.7	60.4	13.2	γPh^{c}—X[38], ωC═O^{b}[30], τPh$^{c}_{trig}$[27]
736	736	731	724	725	724	744	72.4	11.9	84.2	1.0	βPh$^{b}_{symd}$[27], νCCPh^{b}[11], ρC═O^{a}[10]
693		682	701	688	680	691	79.8	25.9	87.5	25.3	γPh$^{c}_{trig}$[66], γPh^{c}—X[23]
575	576	566	558	570	565	567	5.3	123.6	0.4	66.2	δPh^{b}—C—S[19], νC—S[13]

[a]The geometries of the transition dipole moments (β^{μ}, φ^{μ}) and the mean components of the vibrational polarizability tensor (β^{α}, φ^{α}) are reported with respect to a particular mode (B3LYP/SQM-ff/6-31+G(d)). The corresponding frequencies were calculated using B3LYP/SQM-ff/6-31+G(d); PBE/6-31+G(d); ONIOM-PBE/6-31+G(d):PBE/3-21G(d); DMOL3/DNP and QE-PBE/NC-PW:1050eV. Excluding SQM data, all the frequencies are left unscaled.

Spectral Analysis Procedure. The recorded spectra were numerically deconvoluted with the Voigt band profile using PeakFit ver. 4.1 (from Systat Inc., Richmond, CA). The experimental spectrum was assigned on the basis of the corrected SQM results to reduce the DFT systematic errors. Then, the ONIOM and Quantum Espresso results were analyzed by visualizing the normal modes and taking into account the calculated relations of the intensities. In the next step, the DMOL3 calculated frequencies were linked with the related QE ones, based on the normal modes visualization. Finally, the band assignment was refined, taking into account all the results. However, to not lose the consistence of the paper and not to overload the presented data, the presentation of the detailed band assignment in Table 1 has been restricted to the SQM results. The comparison of the calculated frequencies obtained with all the models was given only for the most prominent, best resolved and potentially applicable vibrations, collected in Table 2.

RESULTS AND DISCUSSION

Molecular Properties. The equilibrium geometries obtained with PBE using the quoted models are presented in Figure 1 (a1, b1, and c1). The detailed analysis will be the topic of another paper along with the molecular dynamics study of its conformational properties.[12] All the isolated molecule calculations deliver a similar equilibrium conformation with the biphenyl part twisted for ∼35°. The carbonyl groups, as well as the alkoxy part, lay in the same plane with the adjacent benzene ring. The third ring at the short axis is also twisted with respect to the thioester plane for ∼120°. The perpendicularity of the chiral chain is also a characteristic feature of the studied conformer. When going beyond the isolated molecule model, the ONIOM calculations surprisingly deliver nearly planar biphenyl configuration with the related angle of ∼8°. The third ring is twisted about ∼10° more. The carbonyl group at the chiral part, along with the chiral chain, tends to be out of the adjacent ring's plane for ∼30°. The crystal structure reveals nearly perfect biphenyl planarity. Excluding this part, the geometry of the quoted fragments is generally comparable with the isolated molecule calculations. The solid-state conformation has been perfectly restored by the PBC computations including the biphenyl coplanarity.

To shed light on the interactions driving the studied system, the NCI analysis (recently developed by Yang's group[47]) has been applied. NCI (Non-Covalent Interactions) is a visualization index based on the electron density and its derivatives allowing direct identification of the noncovalent interactions. The method of analysis is conceptually a supplementation of electron localization function (ELF). In general, it is based on the analysis of the reduced density gradient (RDG) at low densities. Differentiation between the noncovalent interactions is based on the analysis of the sign of the second density Hessian eigenvalue times the density. This value is able to characterize the strength of the interaction by means of the density strength and its curvature.[47] The results may be presented as the isosurfaces. In Figure 1 (a2, b2, and c2) the NCI isosurfaces for the intra- and intermolecular interactions are plotted on the studied structures of (a) monomer, (b) cluster, and (c) crystal. The significantly attracting interactions (Coulombic and weak hydrogen-bondings) are visualized in red, whereas the weak van der Waals forces and the repulsive interactions are colorer in green and blue, respectively. The analysis was performed using promolecular densities with the density cutoff = 0.25 using the NCI module implemented in JMOL ver. 12-2-0.[48]

dx.doi.org/10.1021/jp301190z | J. Phys. Chem. A 2012, 116, 7809−7821

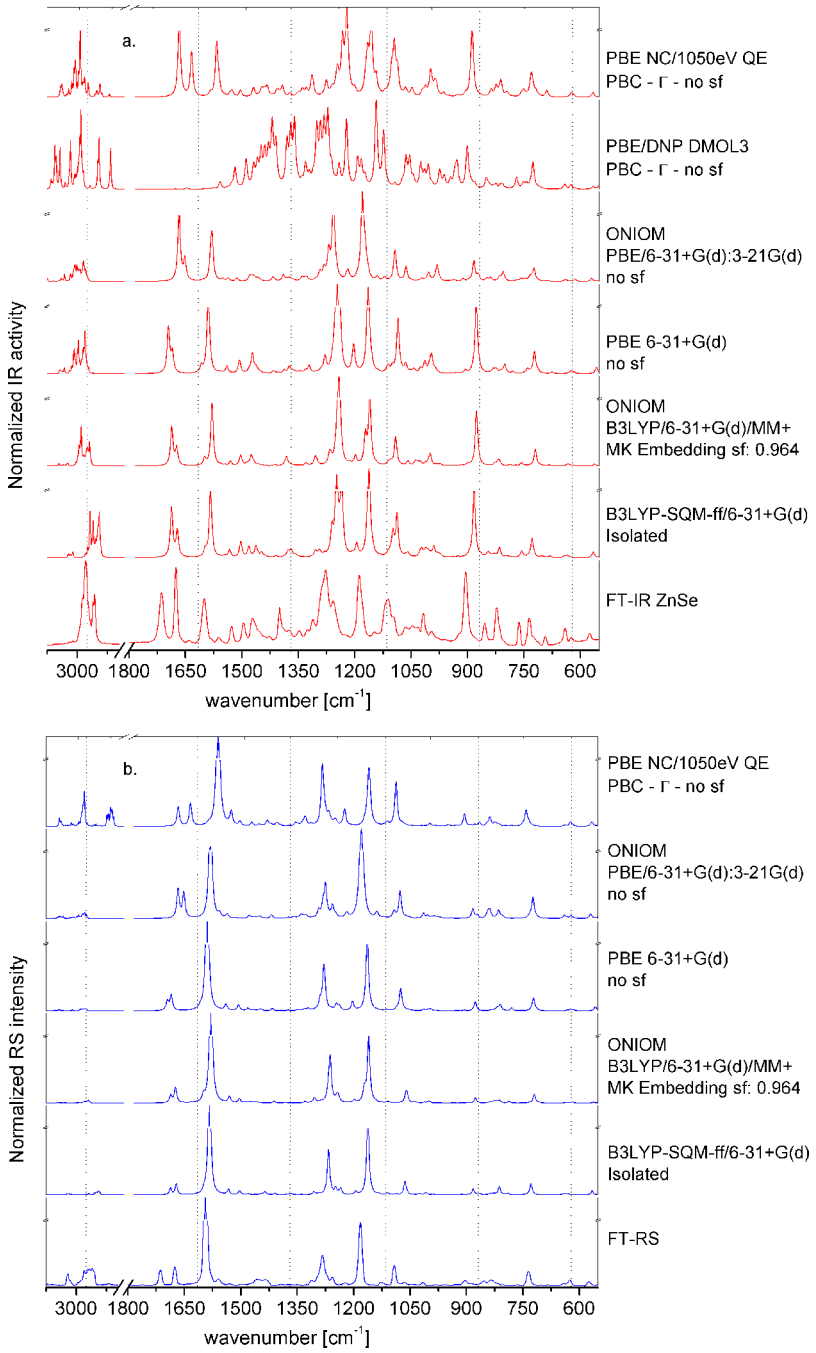

Figure 2. Comparison of the experimental FT-IR (a) and FT-RS (b) spectra of MHPSBO10 along with the improved theoretical ones calculated with the following models: B3LYP/SQM-ff/6-31+G(d); ONIOM-B3LYP/6-31+G(d):MM; PBE/6-31+G(d); ONIOM-PBE/6-31+G(d):PBE/3-21G(d); DMOL3-PBE/DNP; QE-PBE/NC-PW:1050eV.

The NCI analysis clearly shows that only weak intramolecular forces may be expected for the isolated molecule. In the central core, the planarity of the selected fragments is weakly stabilized by the attractions of the hydrogen atoms within the alkoxy and biphenyl parts, as well as by the attractions between the sulfur and oxygen atoms and the adjacent phenyl rings hydrogens. The equilibrium geometry delivered by ONIOM calculations significantly differs from the initial one. Hence, the distribution of the interactions within the optimized cluster is very random. For better transparency, the molecules in the low-layer were hidden in the figure. However, one may see an occurrence of short-range van der Walls interactions (in green) and a rise of weak attractive interactions (in orange) within the environment of the central mesogen. The crystal analysis clearly shows the uniform long-range distribution of the stacking interactions between the phenyl rings. One may also see growing stabilization of the biphenyl coplanarity induced by the hydrogen attractive forces. All the space is mainly covered here by weak attractive interactions. The orange areas indicate the attractions between the hydrogen atoms and π electron clouds which may be treated as very weak hydrogen bonds. It also seems that the carbonyl group related to the chiral part tends to interact more significantly than the second one. Relatively significant forces occurring between the

dx.doi.org/10.1021/jp301190z | J. Phys. Chem. A 2012, 116, 7809−7821

chiral and achiral tails, stabilizing the antiparallel molecular configuration, should also be mentioned.

Vibrational Analysis. *General Discussion of Experimental Spectra.* The experimental FT-IR and FT-RS spectra recorded in both crystal and SmC_A^* phases are presented in Figure S1 (see Supporting Information). To check a possible influence of the ZnSe substrates, the ATR spectrum was additionally recorded for the powder sample. The obtained spectrum does not deliver any noticeable differences, because all the intensities relations are comparable and there is no observable band shifts with respect to the ZnSe sample. The modulated ATR background stems from technical factors. The crystal melting generates relatively visible spectral differences, which are, however, still extremely subtle. The band shifts associated with the phenomenon (collected in Table 1) are very small giving the differences of only few cm^{-1}. Because the spectra were recorded for an unaligned samples, the vibrational intensities distribution is isotropic in both cases, varying very little. It may be seen that the differences manifest more significantly in the IR spectrum, which seems to be more sensitive to the intermolecular forces and the temperature effects disturbing the vibrational spectrum.

The temperature dependent FT-IR studies of the aligned MHPSBO10 samples are the topic of separate paper and will be presented along with the polarized spectra analysis.[11] The present analysis was based on the room temperature spectra, where the bands are sharpest and better resolved, due to absence of reorientational dynamics which occurs in the liquid crystalline state.

The isolated MHPSBO10 molecule exhibit 273 $(3N - 6)$ normal modes. The crystal unit cell built of 186 atoms give rise to 555 $(3N - 3)$ normal modes, which may be theoretically observed via optical vibrational spectroscopy. However, according to the P_{21} point group of the crystal, the frequencies become doubly degenerated, which makes the analysis consistent with the isolated molecule approach. The C_1 symmetry of the isolated molecule allows all the modes to be active in both infrared and Raman spectroscopy. Luckily, the local symmetry of the particular fragments does not lead all the modes to give rise to the spectral intensity, which makes the analysis reliable. The presented analysis was based directly on the computational data which reproduced the experimental results with very good overall accuracy.

Isolated Molecule Calculations. Figures S2 a and b (presented in the Supporting Information), collect the calculated IR and RS spectra. To probe the performance of modern DFT, and choose an appropriate method for the studies beyond the isolated molecule model, over a dozen of popular exchange−correlation functionals were tested in combination with 6-31+G(d,p) basis set. Also the Hartree−Fock calculations were additionally performed. The simplest LDA approach was tested with SVWN. The following GGA functionals were selected: OLYP, BLYP, BP86, and PBE. The modern hybrid functional was chosen as follows: O3LYP, B3LYP, B3P86, PBE0, B1LYP, B3PW91, mPW1PW91. Finally, two new hybrid functionals developed respectively by Grimme's and Thrular's groups, namely wB97XD and M06 were also tested. The latter ones stand out by including some dispersion terms by theory. M06 exhibit raising popularity in the spectroscopy community, giving very promising results.[45,49] The presented spectra were uniformly corrected by appropriate scale factors taken from the literature, despite wB97XD and M06, where the empirically estimated value of 0.95 was applied.[44,49,50]

The FT-IR spectrum is richer in bands, which allows the performance to come to light more clearly. In general, the comparison shows that the worst results were obtained using HF and SVWN. However, when looking at the calculated RS intensities relations, the main spectral features are reproduced quite satisfactorily with SVWN. It should be underlined because LDA was applied here in solid-state calculations to compute the Raman activities of the crystal. Calculations with OLYP and BLYP also did not deliver satisfactory results. B3PW91, B3P86, and PBE0 give very comparable spectra. Calculations with mPW1PW91, wB97XD, and M06 are also of comparable accuracy, and the new generation ones did not deliver any noticeable improvement. The last group also calls for using scale factors closer to 0.95, due to the greater part of Hartree−Fock exchange included by theory. The best results were obtained using namely O3LYP, B1LYP, BP86, PBE, and B3LYP. The performance of hybrid and GGA functionals from the quoted group is very comparable. The advantage of using pure GGA is their wide spreading in all the DFT PBC packages according to relative numerical simplicity. Most often PBE is the functional of the first choice in such methodology. Moreover, using GGA does not require application of drastic scaling procedure, because the corresponding scale factors are very close to 1. It gives a possibility of getting more consistent and comparable spectroscopic calculations, especially when going beyond the isolated molecule approach. Thus, the selection of PBE for more advanced calculations was the obvious choice.

The presented spectra clearly show that none of the functionals could properly restore the separation of the band at ca. 1700 cm^{-1}, which may be assigned to the ν(C═O) stretching vibrations. The most complex and questionable regime includes bands from the range ∼1400−1000 cm^{-1}, linked mainly to the delocalized bending vibrations which are also affected by anharmonicity. To improve the results, the more advanced calculations have been made.

Beyond the Isolated Molecule Approach. Figure 2 presents the vibrational spectra calculated using the above-described models. The isolated molecule calculations performed at the same basis set level both with SQM (using B3LYP) and without any scaling (with PBE), deliver the spectra of very close accuracy. Because most of the vibrations in the middle frequency range are strongly mixed, applying SQM for such complex molecule did not deliver any spectacular changes in the 1400−1000 cm^{-1} range, due to an averaging of the related scale factors. The main advance of using SQM, over all the performed calculations, is the significant improvement of the high frequency regime, because anharmonicity effects are somehow included in the procedure. In all other cases, the calculations could not restore the high frequency spectral features properly.

The simple QM:MM calculations performed for B3LYP did not give any noticeable improvement. However, applying ONIOM calculations with PBE/6-31+G(d)/3-21G(d) influenced the spectrum quite significantly in the middle frequency range with respect to the isolated PBE/6-31+G(d) calculations. It is especially manifested in the Raman spectrum, where the intensities relations are almost perfectly restored. Introducing environmental effects shifts down the ν(C═O) and ν(C═C(Ph)) frequencies, observed at ∼1700 and ∼1600 cm^{-1}. The

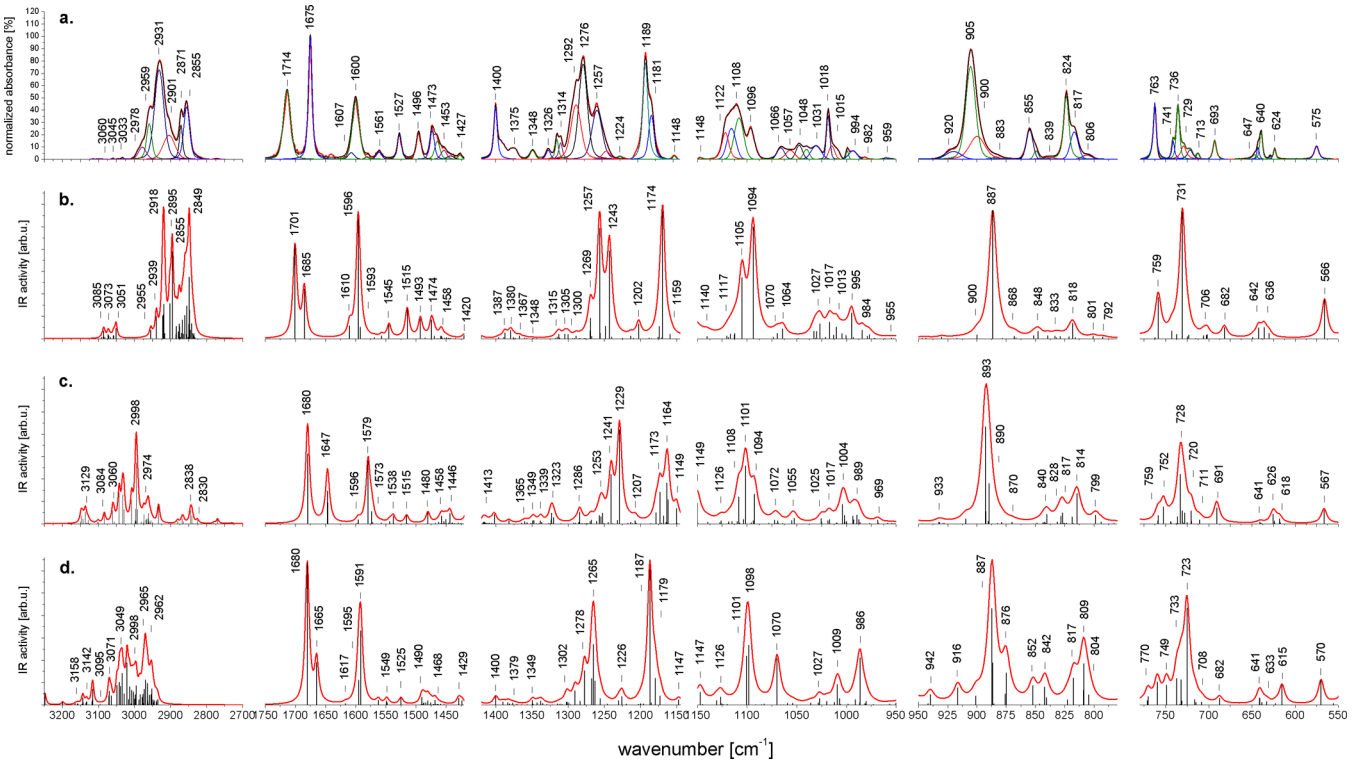

Figure 3. Detailed analysis of the experimental FT-IR (a) spectrum divided into several frequency regimes along with the best theoretical, alternative modeling results obtained with B3LYP/SQM-ff/6-31+G(d) (b), QE-PBE/NC-PW:1050eV (c), and ONIOM-PBE/6-31+G(d):PBE/3-21G(d) (d). The PBE results are left unscaled.

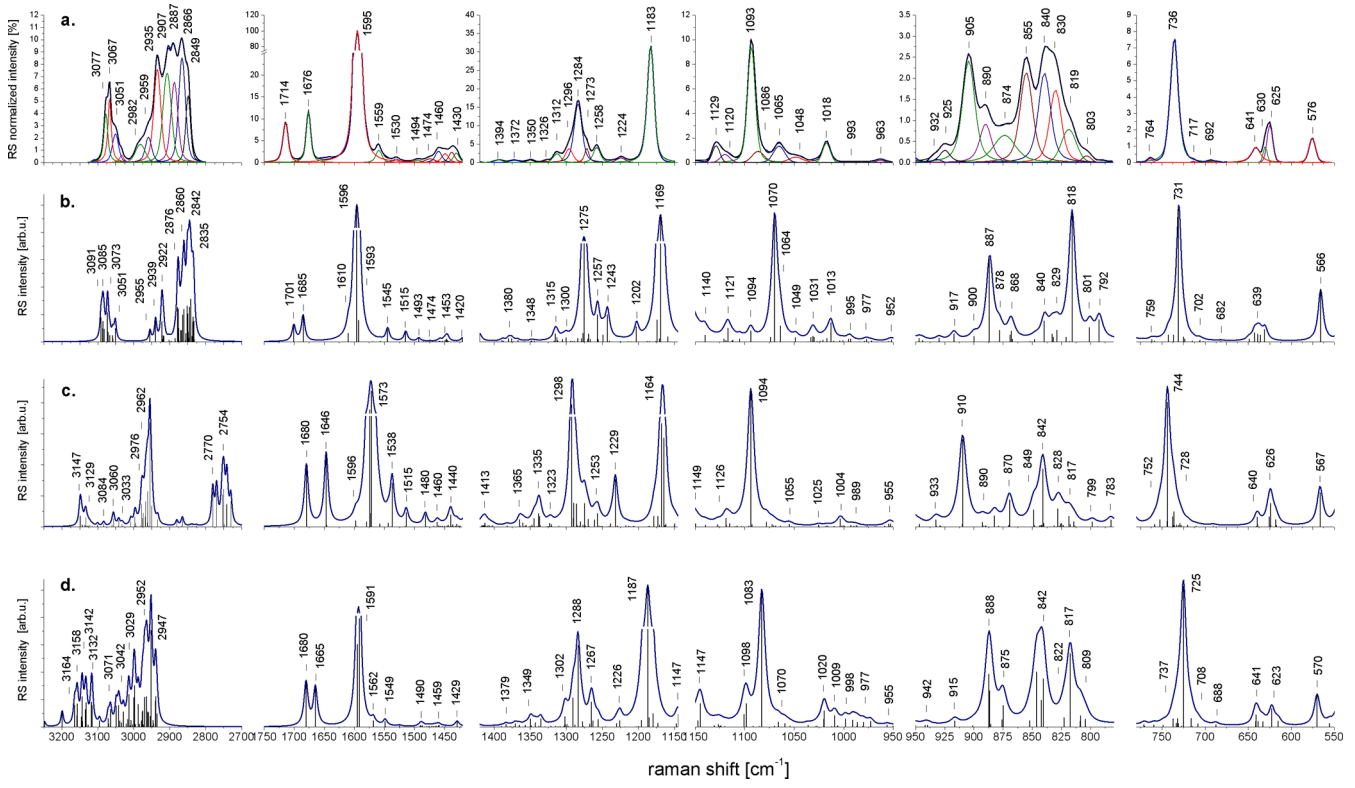

Figure 4. Detailed analysis of the experimental FT-RS (a) spectrum divided into several frequency regimes along with the best theoretical, alternative modeling results obtained with B3LYP/SQM-ff/6-31+G(d) (b), QE-PBE/NC-PW:1050eV (c), and ONIOM-PBE/6-31+G(d):PBE/3-21G(d) (d). The PBE results are left unscaled.

calculations also noticeably changed the intensities relations in the ∼1400−1000 cm^{-1} range.

Introducing periodic boundary conditions delivers further improvement in several cases. As may be seen in Figure 2a, the

dx.doi.org/10.1021/jp301190z | J. Phys. Chem. A 2012, 116, 7809−7821

differential dipole approximation applied for the DMOL3 results completely failed in the studied case. DMOL3 provided good frequencies relation with the other results; however, the lack of the proper intensities description makes the results partially useless. Finally, introducing the DFPT approach solved the crystal intensities problem. As may be seen in Figure 2a, all the main spectral features are properly recovered by the Quantum Espresso calculations. The calculations deliver some improvement in the range of bending vibrations. As mentioned before, we were unable to compute the Raman activities with GGA, because the procedure is not yet implemented in QE. LDA calculations of the Raman spectrum, surprisingly delivered very good results. The only visible weak point is an overestimation of the RS intensities of the bands at ∼1075 and 1275 cm^{-1}. However, the general picture of the simulated vibrational spectrum is very good. It should be underlined that the calculated frequencies in all the spectral regimes are visibly underestimated here. It is hard to unequivocally link the source to this effect. The reason may come from the pseudopotentials and the summation of the GGA errors, as well as from an overestimation of the attractive forces. However, because the present theory level poorly describes the dispersion interactions, the former reason is the most probable. We may conclude that such computations call for using a slight general scaling procedure of ca. 1.015.

Bands Assignments. In Figures 3 and 4 the experimental FT-IR and FT-RS spectra, respectively, are divided into the most characteristic ranges, starting from 3250 cm^{-1} down to 550 cm^{-1}, and presented in details along with the best theoretical results. Table 1 collects the proposed experimental spectrum assignment based on the normal coordinate analysis performed with B3LYP/SQM-ff/6-31+G(d) data. Table 2 presents the most prominent and applicable bands, analyzed in terms of their transition dipole moments and the related vibrational polarizability components (see further text for details), also giving the comparison of related theoretical frequencies calculated with the quoted theoretical models. The selection of the bands applicable for further studies of liquid crystalline compounds must fulfill some conditions. First, the selected band should be of significant intensity, allowing for a reliable analysis. What is more, it should be well resolved and finally cannot be related to various normal modes of different transition moments geometries, or in other words, the band must be well-defined with respect to the transition dipole moment geometry. A studied normal vibration should not be significantly delocalized in the sense of the normal-mode analysis.

Bands at 3250−2700 cm^{-1}. Due to the harmonic approach and lack of the Fermi resonance effects taken into account, the bands in the high frequency range could not be well reproduced by the calculations. Hence, these frequencies are highly overestimated and their energetic ordering is questionable. However, it was possible to empirically resolve and perform interpretation of this regime by using SQM procedure, where the applied scaling factors empirically include the anharmonicity effects. The bands over 3000 cm^{-1} may be assigned to the symmetric (upper bands) and antisymmetric (lower bands) stretching ν_s(CH) vibrations within the phenyl rings. The bands observed at ∼2855 and 2870 cm^{-1} may be assigned to the symmetric stretching modes of the methylene $\nu_{ss}(CH_2)$ and methyl $\nu_{ss}(CH_3)$ groups, respectively. The bands found at ∼2900 and 2930 cm^{-1} were assigned to the antisymmetric $\nu_{ass}(CH_2)$ stretchings. Finally, the bands over ∼2950 cm^{-1} were assigned to the in-plane- and out-of-plane methyl $\nu(CH_3)$ stretching modes.

Bands at 1750−1400 cm^{-1}. MHPSBO10 possesses two carbonyl groups associated with the thioester and the ester parts, respectively. ν(C═O) vibrations along with the ν(C—C) stretching in phenyls are probably the most important normal modes in the context of the ferroelectric liquid crystals studies, due to their reversal vibrational transitions geometry and, hence, their direct application potential in the orientational ordering studies.[1−9] Thus, the proper band assignment is essential in this case. According to the literature, for alkyl thiobenzoates, a ν(C═O) band can be observed in the range ∼1675−1665 cm^{-1}. In the case of phenyl thiobenzoates and its derivatives, the frequency is higher and the band is observed in the range ∼1690−1680 cm^{-1}.[51,52] In this case, the increase of the frequency comes from the inductive effect, caused by the phenyl group. The frequency of the ν(C═O) vibration in benzoates is observed at higher frequencies, over ∼1700 cm^{-1}. Substituting oxygen with sulfur causes the reduction of the force constant, which results from the increased interaction between the electrons from the carbonyl group with the nonbonding pair electron from the sulfur atom. The interaction between the hydrogen atoms from the adjacent phenyl ring with the sulfur atom observed in the NCI analysis also contributes to this effect. Thus, the lower ν(C═O) band, found at 1675 cm^{-1} is assigned to the carbonyl group at the central core. The upper band observed in the solid phase at 1714 cm^{-1} is assigned to the carbonyl group at the chiral part (ν(C*═O)). It is believed that the local dipole moment associated with this molecular fragment underlies the spontaneous polarization phenomenon observed in ferro-/antiferroelectric liquid crystals. Hence, the vibration is of interest to many studies.[1−9]

Table 2 clearly shows the performance in prediction of the quoted frequencies. In the experimental spectra, the carbonyl stretching bands are visibly separated for ∼40 cm^{-1}. All the calculations properly predict the order of the frequencies. However, the calculations within the isolated molecule approach predict the separation to be ∼15 cm^{-1} (i.e., B3LYP) or less (i.e., 9 cm^{-1} by PBE). When going beyond using ONIOM, the separation slightly increases up to 15 cm^{-1} for PBE. However, only the long-range description of the intermolecular interactions with periodic boundary conditions can properly restore the vibrational energy difference. The full electronic DMOL3 calculations predict the difference of 50 cm^{-1}, whereas the QE results give the value 33 cm^{-1}. When comparing the frequencies calculated with PBE using ONIOM with the isolated molecule approach, one can see the reduction of both frequencies. It is hard to unambiguously point the source of this phenomenon. One of the reasons may be the occurrence of the vibrational resonance effects, which may be probed only with a proper description of the long-range Coulombic interactions. This effect may indicate that the C═O oscillators are significantly coupled. However, it also seems that the intermolecular interactions progressively reduce the force constant of the thioester carbonyl group. It is known from the low frequency temperature dependent studies that the biphenyl part lost its planarity upon the crystal melting. However, Table 1 clearly shows that the lower frequency does not vary with the temperature. Thus an influence of the adjacent biphenyl part geometry on the discussed ν(C═O) stretching frequency should be excluded.[12] The upper band progressively shifts up to higher frequencies with an increase of temperature. It may be

linked with a raising dynamics of the chiral part, resulting in an increasing force constant due to the repulsive interactions between the π electrons associated with both the C*═O and the phenyl groups.

The most prominent spectral feature is the presence of the band at ∼1600 cm^{-1}, associated with the phenyl stretching deformations in the central core. However, on the basis of the isolated molecule approach, it is not obvious why the relatively significant difference in the frequency was observed in IR and RS spectroscopy, but only one very strong band was predicted in both cases by the theory. The answer may be delivered only by the solid-state calculations. In fact, the mesogens closed into the antiparralel dimers strongly interact within the central cores, as may be seen in the NCI analysis. Thus, in fact, we should expect two normal modes of the same nature and the different symmetry. While the cores stretch in-phase, we observed the Raman band at 1595 cm^{-1}. The alternative, out-of-phase vibration may be detected with IR at 1600 cm^{-1}. Hence, the interactions cancel the degeneracy and cause the observable frequency shift (5 cm^{-1}), which may be properly restored by both DMOL3 and QE computations (6 cm^{-1}), as may be seen in Table 2. This effect supports the assumption that the most significant interactions take place within the central cores of the mesogens.

Another characteristic band may be observed at ∼1530 in both spectroscopies. The band was assigned to the rocking in plane vibration ρPh-H of the biphenyl core, mixed with its stretching ν(C−CPh) normal mode. The range down to 1400 cm^{-1} is covered by the scissoring vibrations $\delta(CH_2)$ of methylene groups, giving broadened, overlaying bands, of which proposed assignment is presented in Table 1.

Calculations with Quantum Espresso significantly improved the discussed, probably the most important frequency range; however, the systematic underestimation of the calculated frequencies in magnitude of ca. ∼20−30 cm^{-1} should be noticed.

Bands at 1400−950 cm^{-1}. The discussed range is alternately staggered by the deformations of the phenyl rings, mostly of rocking type, and by the deformations of the alkyl groups with the following order: $\omega(CH_2) \rightarrow \tau(CH_2) \rightarrow \rho(CH_2)$. Moreover, most of the vibrations are significantly mixed. Hence, the discussed range is problematic from the theoretical point of view, because the calculations generate deviations of ∼20 cm^{-1}. Thus, the analysis of this spectral range may be somehow arbitrary. For such a complex molecule the precision of a few cm^{-1} would be needed. Moreover, as shown by the NCI analysis, the relatively significant intermolecular forces attract the fragments which mutually contribute to the discussed normal modes. Finally, the experimental peak picking may be performed approximately here. However, some of the most prominent spectral features were clearly restored by the computations.

In the FT-IR spectrum one may see an intensive band at ∼1190 cm^{-1}. The overlapping shoulder may also be visible. Thus, the deconvolution delivers two bands at 1189 and 1181 cm^{-1}. The vibration manifesting as the lower band also exhibits strong Raman activity, observed at 1183 cm^{-1}. The former band has been assigned to the phenyl ring rocking mode deforming the ester bridge in the chiral part (ρPh^c−X[73%], $\nu CCPh^c$[21%]). The latter may be associated with the similar vibration related to the thioester bridge ($\rho Ph^{a,b}$−X[38%], vPh^b−C[23%], $\nu CCPh^b$[14%], δPh^b_{trigd}[5%]). As may be seen in Table 2, the applied methods predict the frequency very randomly. However, the best relation of the intensities was delivered by ONIOM approach, which also seems to give the best reproduction of the ∼1280 cm^{-1} features in both spectroscopies. Hence, the SQM assignment was refined taking the results into account.

The set of overlapping bands was observed in the FT-IR spectrum also at ∼1110 cm^{-1} with the most prominent component at 1106 cm^{-1}. The band has been assigned also to the ν(C−O) in the ester part and to the rocking of the interacting C−H groups in the adjacent phenyl ring.

The intensive Raman band observed at 1093 cm^{-1} is associated with the ν(S−Ph) stretching vibration.

Bands at 950−550 cm^{-1}. The most prominent band was observed at 905 cm^{-1} in FT-IR spectroscopy and may be assigned to the rocking deformation of the thioester group significantly coupled with the ν(C—S). Some background calculations,[14] performed with the strong electric fields applied to the mesogenic core, indicated that this vibration is sensitive to the Coulombic interactions and the electron density distribution within the central core, which affect the C—S bond length. Elongation of this bond is reflected by the frequency shifts toward the lower wavenumbers. Although the effect observed in Table 1 is weak, it may be directly related to this effect, which is opposite to the one observed for ν(C═O) and ν(C*═O) normal modes. The corresponding Raman band of medium intensity overlaps with the others. Although the intensity of the IR band was perfectly predicted by QE calculations, the related RS intensity is strongly underestimated, improperly suggesting assigning the mode at 910 cm^{-1}. However, the practical applicability of the RS spectrum in this range is questionable.

Out of plane phenyl vibration mixed with the wagging of the carbonyl group at the chiral part (γPh^c—X[38%], ωC═O^b[30%], γPh^c_{trig}[27%]) manifests as the well resolved band of medium intensity in the FT-IR spectrum at 763 cm^{-1}. The band was properly predicted by the theory. However, beyond the isolated molecule model, some other features have risen near the predicted frequency, which does not stay in agreement with the experimental results. The mode exhibit negligible intensity in the FT-RS spectrum. Another well resolved band may be probed with RS spectroscopy at 736 cm^{-1}. The band is connected strictly with the out of plane vibration of the quoted phenyl ring (τPh^c_{trig}[66%], γPh^c—X[23%], ωC═O^b[8%]). The band is also present, however not well resolved in FT-IR. The QE calculations failed here in the prediction of the related IR activity.

Finally, the presence of the well resolved δ(C−S−C) band at 576 cm^{-1} should also be noticed.

Vibrational Transition Moments Geometry. To get the geometry of the transition dipole moments and the main components of the vibrational polarizability tensors, the IOP(7/33=1) command was imposed in G09. The geometries were determined in terms of the molecular frame with respect to the molecular long axis defined as the lowest component of the calculated moment of inertia tensor as presented in Figure 5. The calculated geometries of both IR and RS vibrational transition moments are collected in Table 2. The presented geometries are useful for further orientational studies of the aligned samples with the anisotropic transition moments distribution.

dx.doi.org/10.1021/jp301190z | J. Phys. Chem. A 2012, 116, 7809−7821

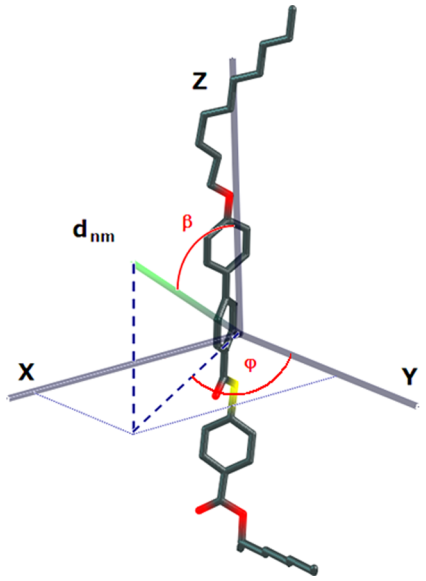

Figure 5. Scheme of the angles defining the vibrational transition moment within the molecular frame as defined by the main components of the moment of inertia tensor. The molecular long and short axes line up with the *Z* and *Y* components, respectively. Presented transition dipole moment corresponds to the ν(C*═O) normal mode calculated with B3LYP/6-31+G(d).

CONCLUSIONS

The vibrational spectrum of MHPOSBO10 in the middle frequency range have been reported and interpreted in details. The performance of modern DFT functional has been probed and very good accuracy of the relatively simple PBE functional has been confirmed. The environmental effects were analyzed in terms of NCI analysis. Affords of improving the theoretical vibrational spectra have been undertaken. Several modern quantum-chemical models were tested and very good performance of density functional perturbation theory in the description of big sized molecular crystals has been shown. The calculations for such a large molecular system have been reported here for the first time. The presented results are very promising. Their quality encourages studying related size systems, driven by middle strength interactions like other liquid crystalline systems, polymers, or medicinal drugs. The normal-mode analysis, along with the transition dipole moments and vibrational polarizability components, has been given. The presented results delivered good basis for further spectroscopic studies of the aligned MHPSBO10 samples, which are in progress and will be presented soon.

ASSOCIATED CONTENT

Supporting Information

Comparison of the experimental spectra, atom numbering, test of exchange−correlation functionals, definitions of local symmetry coordinates, complete normal-mode analysis. This information is available free of charge via the Internet at http://pubs.acs.org.

AUTHOR INFORMATION

Corresponding Author

*E-mail: druzbick@chemia.uj.edu.pl.

Notes

The authors declare no competing financial interest.

ACKNOWLEDGMENTS

We give our appreciation to Malgorzata Barańska, Ph.D. D.Sc., Katarzyna Chruszcz-Lipska, Ph.D., and Tomasz Wróbel M.Sc. from the Department of Chemical Physics, Jagiellonian University, Poland, for the access to the Raman and ATR spectrometers and their support in the measurements. The kind help of Dr. Mariusz Sterzel Ph.D. (PL-Grid, Cracow, Poland) and Professor Paolo Gianozzi (Department of Physics, University of Udine, Italy) in modifying QUANTUM ESPRESSO v 4.3.2 is also acknowledged. We are very grateful to Professor Tom Sundius (Department of Physical Sciences, University of Helsinki, Finland) for providing the MOLVIB program. K.D. gives his big appreciation to Damian G. Allis, Ph.D. (Department of Chemistry, Syracuse University, USA), and Witold Piskorz, Ph.D. (Department of Inorganic Chemistry, Jagiellonian University, Poland), for stimulating discussions and the inspiration in the field of solid-state computations. This research was supported in part by PL-Grid Infrastructure (Grant ID: druzbicki, Zeus Supercomputer). The computations were also done in part at the Academic Computer Centre CYFRONET AGH, Cracow, Poland (Grants ID: MNiSW/SGI3700/UJ/007/2009, Baribal Supercomputer; MNiSW/IBM_BC_HS21/UJ/032/2009, Mars Supercomputer). Calculations with Materials Studio 5.5 were performed within the Accelrys Polish national license.

REFERENCES

(1) Kocot, A.; Vij, J. K.; Perova, T. S. *Advances in Liquid Crystals*; John Wiley & Sons: New York, 2000; Vol. *6*, pp 203−269.
(2) Ossowska-Chruściel, M. D.; Korlacki, R.; Kocot, A.; Wrzalik, R.; Chruściel, J.; Zalewski, S. *Phys. Rev. E* **2004**, *70*, 041705(1)−041705(10).
(3) Korlacki, R.; Fukuda, A.; Vij, J. K.; Kocot, A.; Görtz, V.; Hird, M.; Goodby, J. W. *Phys. Rev. E* **2005**, *72*, 041704(1)−041704(9).
(4) Kocot, A.; Vij, J. K. *Liq. Cryst.* **2010**, *37*, 653−667.
(5) Hayashi, N.; Kato, T.; Aoki, T.; Ando, T.; Fukuda, A.; Seomun, S. S. *Phys. Rev. E* **2002**, *65*, 041714(1)−041714(11).
(6) Hayashi, N.; Kato, T.; Kocot, A.; Fukuda, A.; Vij, J. K.; Heppke, G.; Kwada, S.; Kondoh, S. *Phys. Rev. E* **2006**, *74*, 051706(1)−051706(11).
(7) Kim, K. H.; Takanishi, Y.; Ishikawa, K.; Takezoe, H.; Fukuda, A. *Liq. Cryst.* **1994**, *16*, 185−202.
(8) Cheng, J.; Cheng, Y.; Ruan, W.; Xu, W.; Zhao, B.; Zhang, G. *J. Chem. Phys.* **2005**, *122*, 214913(1)−214913(8).
(9) Zhao, J. G.; Yoshihara, T.; Siesler, H. W.; Ozaki, Y. *Phys. Rev. E* **2001**, *64*, 031704(1)−031704(10).
(10) Drużbicki, K.; Mikuli, E.; Ossowska-Chruściel, M. D. *Vibr. Spectrosc.* **2010**, *52*, 54−62.
(11) Drużbicki, K.; Kocot, A.; Mikuli, E.; Ossowska-Chruściel, M. D.; Chruściel, J. *J. Phys. Chem. B.*, submitted for publication.
(12) Drużbicki, K.; Mikuli, E.; Łasocha, W. To be published.
(13) Ossowska-Chruściel, M. D.; Chruściel, J. *Thermochim. Acta* **2010**, *502*, 51−59.
(14) Drużbicki, K.; Mikuli, E.; Zalewski, S.; Ossowska-Chruściel, M. D.; Chruściel, J.; Czerwiec, J. M. *Mater. Chem. Phys.*, submitted for publication.
(15) Ossowska-Chruściel M. D. et al. To be published.
(16) Sun, H. *J. Phys. Chem. B* **1998**, *102*, 7338−7364.
(17) *Materials Studio 5.5*, Accelrys Software Inc., 2001−2011.
(18) Frisch, M. J.; et al. *Gaussian 09*, Revision B.1; Gaussian, Inc.L Wallingford, CT, 2009.
(19) Becke, A. D. *J. Chem. Phys.* **1993**, *98*, 5648−5652.
(20) Lee, C.; Yang, W.; Parr, R. G. *Phys. Rev. B.* **1988**, *37*, 785−789.
(21) Vosko, S. H.; Wilk, L.; Nusair, M. *Can. J. Phys.* **1980**, *58*, 1200−1211.

(22) Stephens, P. J.; Devlin, F. J.; Chabalowski, C. F.; Frisch, M. J. *J. Phys. Chem.* **1994**, *98*, 11623−11627.
(23) Korlacki, R.; Merkel, K.; Vij, J. K.; Wrzalik, R.; Kocot, A.; Ossowska-Chruściel, M. D.; Chruściel, J.; Zalewski, S. *Liq. Cryst.* **2006**, *33*, 219−225.
(24) Sundius, T. *J. Mol. Struct.* **1990**, *218*, 321−326.
(25) Sundius, T. *Vibr. Spectrosc.* **2002**, *29*, 89−95.
(26) Pulay, P.; Fogarasi, G.; Pongor, G.; Boggs, J. E.; Vargha, A. *J. Am. Chem. Soc.* **1983**, *105*, 7037−7047.
(27) Dapprich, S.; Komaromi, I.; Byun, K. S.; Morokuma, K.; Frisch, M. J. *J. Mol. Struct. (THEOCHEM)* **1999**, *1*, 461−462.
(28) Perdew, J. P.; Burke, K.; Wang, Y. *Phys. Rev. B* **1996**, *54*, 16533−16539.
(29) Perdew, J. P.; Burke, K.; Ernzerhof, M. *Phys. Rev. Lett.* **1996**, *77*, 3865−3868.
(30) Fabri, C.; Szidarovszky, T.; Magyarfalvi, G.; Tarczay, G. *J. Phys. Chem. A* **2011**, *115*, 4640−4649.
(31) Zhurko, G. *Chemcraft*, http://www.chemcraftprog.com.
(32) Delley, B. *J. Chem. Phys.* **1990**, *92*, 508−517.
(33) Delley, B. *J. Chem. Phys.* **2000**, *113*, 7756−7764.
(34) Clark, S. J.; Segall, M. D.; Pickard, C. J.; Hasnip, P. J.; Probert, M. J.; Refson, K.; Payne, M. C. *Z. Kristallogr.* **2005**, *220*, 567−570.
(35) Giannozzi P. et al. *QUANTUM ESPRESSO*, http://www.quantum-espresso.org.
(36) Allis, D.; Prokorova, D. A.; Korter, T. *J. Phys. Chem. A* **2006**, *110*, 1951−1959.
(37) Fitzgerald, G. https://community.accelrys.com/servlet/JiveServlet/download/8221-3855/Cell_MkHessian.pl.zip.
(38) Canepa, P.; Hanson, R. M.; Ugliengo, P.; Alfredsson, M. *J. Appl. Crystallogr.* **2011**, *44*, 225−229.
(39) Canepa, P. *J-ICE*, http://j-ice.sourceforge.net/.
(40) Baroni, S.; Giannozzi, P.; Isaev, E. *Rev. Mineral. Geochem.* **2010**, *71*, 39−57.
(41) http://www.sas.upenn.edu/rappegroup/htdocs/Research/psp_gga.html.
(42) Dal Corso, A. ATOMIC CODE (QE distribution), http://qe-forge.org/projects/pslibrary/.
(43) Perdew, J. P.; Zunger, A. *Phys. Rev. B* **1981**, *23*, 5048−5079.
(44) Gianozzi, P. Private communication, http://www.democritos.it/pipermail/pw_forum/.
(45) Schaftenaar, G.; Noordik, J. H. *J. Comput.-Aided Mol. Design* **2000**, *14*, 123−134.
(46) http://boson5.phys.tku.edu.tw/mhl/opium-Vps/reports_20081231/.
(47) Johnson, E. R.; Keinan, S.; Mori-Sánchez, P.; Contreras-García, J.; Cohen, A. J.; Yang, W. *J. Am. Chem. Soc.* **2010**, *132*, 6498−6506.
(48) *J-Mol*, http://wiki.jmol.org/index.php/Main_Page.
(49) Helios, K.; Wysokiński, R.; Pietraszko, A.; Michalska, D. *Vibr. Spectrosc.* **2011**, *55*, 207−215.
(50) Merrick, J. P.; Moran, D.; Radom, L. *J. Phys. Chem. A* **2007**, *111*, 11683−11700.
(51) Nyquist, R. A. *Interpreting Infrared, Raman and Nuclear Magnetic Resonance Spectra*; Elsevier: Amsterdam, 2001.
(52) Wojtkowiak, B.; Chabanel, M. *Molecular Spectroscopy*; PWN: Warsaw, Poland, 1992.